

Sensing vibrations using quantum geometry of electrons

Bhuvanewari R. ^{1,2,*}, Mandar M. Deshmukh ^{3,†} and Umesh V. Waghmare^{1,‡}

¹*Theoretical Sciences Unit, Jawaharlal Nehru Centre for Advanced Scientific Research, Bangalore 560064, India*

²*School of Electrical and Electronics Engineering, SASTRA Deemed University, Thanjavur 613401, India*

³*Department of Condensed Matter Physics and Materials Science, Tata Institute of Fundamental Research, Mumbai 400005, India*



(Received 22 February 2024; revised 19 June 2024; accepted 28 June 2024; published 12 July 2024)

We show that the coupling of phonons with electrons can have nontrivial consequences to the quantum geometry of an electronic structure, which manifests as oscillations in the Berry curvature dipole and hence have observable nonlinear Hall signatures. Using these, we introduce a vibrational spectroscopy based on the geometry of quantum electronic structure (GQuES) making specific predictions for the transport and radiative GQuES spectra of two-dimensional materials. The selection rule presented here for the GQuES activity of a phonon allows the measurement of acoustic and optic phonons spanning sub-GHz, THz, and infrared frequencies, and is readily generalized to other dynamical excitations. GQuES can be used even for materials having trivial quantum electronic geometry, such as hexagonal boron nitride, through a proximal interaction with substrates such as graphene.

DOI: [10.1103/PhysRevB.110.014305](https://doi.org/10.1103/PhysRevB.110.014305)

I. INTRODUCTION

When the external parameters or fields interacting with a quantum system change slowly along a cyclic path or a loop, its quantum energy state time-evolves adiabatically, picking up two phase factors: (i) the dynamical phase factor determined by the energies of quantum states traversed during the cyclic evolution and (ii) an additional factor that depends only on the geometry of quantum states accessed along the loop in the parameter space, as shown by Berry in 1984 [1]. When these parameters correspond to dynamical variables of slow degrees of freedom, the geometric or Berry phases are physically relevant to measurable properties significant to applications [2]. The manifestation of Berry phases is omnipresent and has been realized in diverse phenomena in quantum chemistry, physics, and material science [2]. In the last two decades, Berry phases and curvature have been shown to govern the electronic topology of crystals that defines quantum states of matter such as topological insulators, and Dirac and Weyl semimetals [3,4].

In this paper, we propose a vibrational spectroscopy technique based on the ideas of Berry phases and curvature as the quantum geometric properties of electrons. This spectroscopy combines the capabilities of Brillouin, Raman, and IR spectroscopies in the sense it allows the measurement of frequencies of acoustic and optic phonons. In analogy with surface-enhanced Raman scattering, it can be used even in the analysis of systems with trivial quantum geometry by bringing them in proximity to a substrate with nontrivial quantum geometry.

The bending of the electronic trajectory in a crystal due to the Berry curvature of its quantum electronic structure causes an electrical Hall effect even in the absence of a magnetic field [2,5]. Such a linear anomalous Hall effect [6] is observable only in systems with broken time-reversal symmetry. The electronic Berry curvature dipole, a first moment of Berry curvature, was shown theoretically to result in nonlinear Hall (NLH) effects [7], which have been observed in the time-reversal symmetric systems [8], probing the quantum geometry of materials, particularly those exhibiting a narrow band gap and low crystallographic symmetry [9].

We demonstrate that dynamical excitations lower the symmetry of a crystal and induce an oscillating Berry curvature dipole. Its signatures in the frequency-dependent Hall response constitute a powerful geometry of the quantum electronic structure (GQuES)-based spectroscopic tool to measure the excitation spectrum. Using first-principles theory and simulations, we illustrate the GQuES tool with crystal specific predictions for experimental measurements of Hall transport and THz/IR emission to probe the frequencies of acoustic and optic phonons.

In the theoretical demonstration here, we choose two-dimensional (2D) crystals. An ultrathin 2D crystal retains its intrinsic carrier mobility when used as a channel in a field-effect transistor, because of the dangling-bond free structure [10] and offers superior electrostatic control over its charge carriers through the gate voltage [11]. 2D crystals with distinct electronic properties can be integrated [12] into heterostructures to enable multifunctionality and ease in the fabrication of low powered electronic devices with enhanced performance [13]. Noting the advantage in the experimental realization and interesting quantum geometry exhibited by some of the 2D materials [8], we consider the readily available 2D materials, monolayered tungsten telluride (WTe₂) and aligned graphene-hexagonal boron nitride (gr-hBN) in our analysis to facilitate experiments.

*Contact author: bhuvana@jncasr.ac.in

†Contact author: mandar.m.deshmukh@gmail.com

‡Contact author: waghmare@jncasr.ac.in

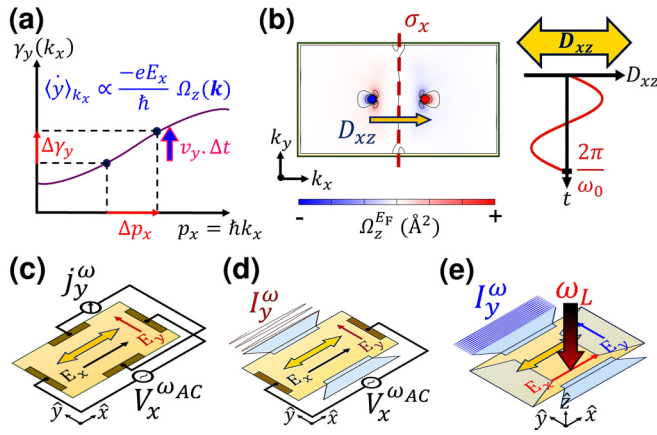


FIG. 1. Quantum geometric origin of the anomalous Hall velocity and vibrational spectroscopy. Transverse velocity $\langle \dot{y} \rangle_{k_x}$ of an electron (a) driven by a force $F_x = -eE_x$ along the \hat{k}_x direction is associated with the change in its Berry phase γ_y generated by the Berry curvature $\Omega_z(\mathbf{k})$. T_d -WTe₂ monolayer exhibits nontrivial $\Omega_z(\mathbf{k})$ and finite Berry curvature dipole D_{xz} , due to its mirror symmetry σ_x (b). A GQuES-active vibrational mode at frequency ω_0 dynamically lowers its symmetry, permitting oscillations in D_{xz} [highlighted by the double-headed yellow arrow in the right subpanel of (b)]. A schematic of an electronic device (c) proposed for GQuES-based transport spectroscopy measures the transverse current j_y^ω in response to an applied voltage $V_x^{\omega_{ac}}$ at low frequency ($\omega_{ac}, \omega_0 < 10$ GHz), originating from D_{xz} and its oscillations. A schematic of the device proposed for GQuES-based emission/optical spectroscopy measures the intensity of emitted radiation I_y^ω polarized with electric field E_y in response to an applied voltage $V_x^{\omega_{ac}}$ (d) or incident light of frequency $\omega_L \geq \omega_0$ polarized along the \hat{x} direction (e) when ω_0 is in THz.

II. THEORY

The energy eigenfunction of an electron in a crystal, labeled by the Bloch wave vector $\mathbf{k} \in$ Brillouin zone (BZ), is $\psi_{\mathbf{k}} = e^{i\mathbf{k}\cdot\mathbf{r}} u_{\mathbf{k}}(\mathbf{r})$ with $u_{\mathbf{k}}$ being cell-periodic. As $\psi_{\mathbf{k}}$ is periodic in k space, its adiabatic evolution across BZ is cyclic and picks up a geometric phase [1], $\gamma_\alpha = i \oint dk \langle u_{\mathbf{k}} | \frac{\partial}{\partial k_\alpha} | u_{\mathbf{k}} \rangle$, where α denotes the direction in momentum space (we do not include the band index for simplicity). The integrand is the Berry connection $A_\alpha(\mathbf{k})$ and the Berry curvature is $\Omega_\delta(\mathbf{k}) \equiv \varepsilon_{\delta\beta\alpha} \frac{\partial}{\partial k_\beta} A_\alpha(\mathbf{k})$, which is analogous to a magnetic field governing the trajectory of electronic motion in reciprocal space [1]. $\Omega_\delta(\mathbf{k})$, the curvature of quantum geometry of electrons in 2D, is nonzero only along the \hat{z} direction ($\delta = z$) and vanishes identically in a crystal with time-reversal and inversion symmetries.

However, $\Omega_z(\mathbf{k})$ can be nonzero in low-symmetry 2D crystals and gives rise to anomalous velocity v_y , perpendicular to the motion driven by the electric force $F_x = -eE_x$, due to a shift in $\gamma_y \propto \langle \dot{y} \rangle$ [see the semiclassical picture in Fig. 1(a)]. This transverse velocity causes an anomalous Hall current and the conductivity is $\sigma_{xy} = \frac{e^2}{\hbar} \iint \frac{d^2\mathbf{k}}{(2\pi)^2} \Omega_z(\mathbf{k}) f(\varepsilon_{\mathbf{k}})$, where $f(\varepsilon_{\mathbf{k}})$ is the Fermi-Dirac distribution [14].

In a 2D time-reversal symmetric crystal $\Omega_z(\mathbf{k}) = -\Omega_z(-\mathbf{k})$, and a linear anomalous Hall effect is not possible as $\sigma_{xy} = 0$. However, an applied field E_x shifts the Fermi surface in k space, giving an *asymmetric* nonequilibrium distribution of electrons [15] (see Supplemental Material [16]

and also references therein [17–28] for details of the calculations). It causes a *nonlinear* Hall current that depends quadratically on E_x and is determined by the Berry curvature dipole D [7]. $j_y \propto D \cdot E_x^2$, where

$$D = \iint_{\mathbf{k}} \left[\frac{\partial}{\partial k_x} \Omega_z(\mathbf{k}) \right] f(\varepsilon_{\mathbf{k}}) \quad (1a)$$

$$= -\frac{1}{\hbar} \iint_{\mathbf{k}} [v_x(\mathbf{k})] \left[\frac{\partial}{\partial \varepsilon_{\mathbf{k}}} f(\varepsilon_{\mathbf{k}}) \right] \Omega_z(\mathbf{k}). \quad (1b)$$

Noncentrosymmetric Weyl semimetals (WSMs) are good candidates to exhibit the NLH effect, as a consequence of large $\Omega_z(\mathbf{k})$ arising near the Weyl points that act as magnetic monopoles [29,30]. In response to an ac electric field $E_x(t) = \text{Re}(\mathcal{E}_x \cdot e^{i\omega_{ac}t})$, the symmetry-allowed D generates a NLH current at twice the applied frequency $j_y(2\omega_{ac})$ and at zero frequency $j_y(0)$ [7]. A second-order NLH effect was first observed in the WTe₂ bilayer [8], and the strong NLH responses in the transport signatures were traced back to its tilted band anticrossings, using a 2D massive Dirac model [31]. In addition, electrically switchable D was demonstrated in the T_d -WTe₂ monolayer (type-II WSM) [32]. Gao *et al.* [33] derived a field correction to the Berry curvature and proposed a gauge-invariant Berry connection polarizability, which can be associated with a nonlinear *anomalous* Hall effect in systems with both time-reversal and inversion symmetries [34].

Nonzero $\Omega_z(\mathbf{k})$ and D (D_{bz} with $b = x, y$) are constrained by the symmetries of the crystal (see Supplemental Material [16]). For example, consider a 2D crystal having only the σ_x reflection symmetry [shown in Fig. 1(b)]. Since $\Omega_z(\mathbf{k})$ is odd under the time-reversal and $\sigma_x(k_x, k_y) \rightarrow (-k_x, k_y)$ symmetries, its D_{xz} is nonzero and its magnitude is determined by $\Omega_z(\mathbf{k})$ and the group velocity of electrons at the Fermi energy [7]. On the other hand, D_{yz} of such a crystal vanishes as the velocity along the \hat{y} direction is even under the reflection symmetry σ_x . A single mirror symmetry (σ_x or σ_y) of a 2D crystal permits nonzero D , perpendicular to the mirror line (D_{xz} or D_{yz}) [Fig. 1(b)].

In this paper, we use the idea that the symmetry of a structure can get lowered during a normal mode of vibration (frequency ω_0), allowing oscillations in D [right subpanel of Fig. 1(b)]. This naturally causes an observable NLH response modulated with frequency ω_0 . Expanding up to first order in u , $D = D^{(0)} + u \frac{\partial D}{\partial u} \Big|_{u=0}$ where $u = u_0 \cos(\omega_0 t)$. Within a relaxation time approximation, the frequency-dependent NLH current is

$$j_y(\omega) = -\frac{\epsilon_{abc} e^3 \tau}{4(1 + i\omega\tau)} \mathcal{E}_x^2 \left\{ 2D[\delta(\omega - 2\omega_{ac}) + \delta(\omega)] \right. \\ \left. + u_0 \frac{\partial D}{\partial u} \Big|_{u=0} [\delta(\omega - (\omega_0 + 2\omega_{ac})) \right. \\ \left. + \delta(\omega - |\omega_0 - 2\omega_{ac}|) + 2\delta(\omega - \omega_0)] \right\}, \quad (2)$$

where e and τ are the electronic charge and relaxation time, respectively. For a 2D crystal with an inherent D , both the terms contribute to the NLH current: the first one at (i) $\omega = 0$ (rectification), (ii) $2\omega_{ac}$ (second harmonic

generation), which have been observed [8], and the second one, *yet to be observed*, at (iii) $\omega = \omega_0$ and (iv) $\omega = |\omega_0 \pm 2\omega_{ac}|$. Thus, $\partial D/\partial u \neq 0$ defines the selection rule for GQuES spectroscopy and for only the $q=0$ ($\lambda \rightarrow \infty$) phonon, $\frac{\partial D}{\partial u} \neq 0$, because of the conservation of momentum [35], and $\frac{\partial D}{\partial u_{q \neq 0}} = 0$. We expect the temperature dependence of spectral peaks in Eq. (2) to arise primarily from the Bose-Einstein distribution function, which will be taken up in future work based on a fully quantum mechanical analysis of GQuES spectroscopy.

When the symmetries of a 2D crystal force its intrinsic D to vanish, only the second term containing $\partial D/\partial u$ is responsible for the NLH current peaking at frequencies ω_0 and $|\omega_0 \pm 2\omega_{ac}|$. It can be measured as ω -dependent Hall voltage [Fig. 1(c)], which is feasible for low-frequency vibrations (for example, acoustic phonons). As ω_0 of an optical phonon is typically in THz, its transport measurement in a circuit is challenging [Fig. 1(c)], and may rather be detected as THz radiation with polarization E_y emitted by the sample aided with a transverse antenna structure [Fig. 1(d)]. GQuES-based optical spectroscopy is also possible with lasers [Fig. 1(e)], which involves normal incidence of light with E_x polarization at frequency ω_L (THz) and the detection of emitted electromagnetic radiation with E_y polarization peaking at frequencies $2\omega_L \pm \omega_0$.

III. PREDICTIONS: MATERIAL-SPECIFIC GQuES SPECTRA

We now present material-specific evidence to support these ideas using first-principles theoretical calculations. The T' -WTe₂ monolayer, a 2D quantum spin system [36], belongs to the centrosymmetric $P21/m$ space group. Though bulk WTe₂ (a type-II WSM) belongs to the $Pmn2_1$ space group and hosts nontrivial Berry curvature near the Weyl points due to the lack of inversion symmetry of its structure [37], a centrosymmetric T' -WTe₂ monolayer forces its overall intrinsic Berry curvature (and hence D) to vanish. However, the distortions induced by a B_u vibrational mode at $\omega_0 = 3.74$ THz [Fig. 2(a)] lower its symmetry to a single mirror plane σ_x and permit nonzero D_{xz} [Fig. 2(b)], induced orthogonal to the σ_x mirror line.

A sizable $\Omega_z(\mathbf{k})$, of the order of few 100 \AA^2 , concentrated near the Weyl points (WPs), oscillates in its polarity as the T' -WTe₂ structure vibrates with the B_u mode [see the insets of Fig. 2(b)]. Though the induced D at Fermi energy (E_F) is of the order of 10^{-1} \AA , it is the sensitivity of D with respect to the amplitude of a specific vibrational mode that is relevant to GQuES. Noting that B_u is a polar phonon and can be selectively excited with IR radiation at a frequency of ~ 3.74 THz, we expect its GQuES Hall signal to get enhanced systematically with the IR pump, though it is not necessary. This is somewhat similar to the metastable topological phases of HgTe obtained through the coherent excitation of an IR-active phonon mode [38].

A long wavelength ($q \rightarrow 0$) longitudinal acoustic (LA) phonon [Fig. 2(a)] is a quantized form of a strain wave [right subpanel of Fig. 2(a)]. It also induces oscillations in D [Fig. 2(b)] as the associated uniaxial strain along the y

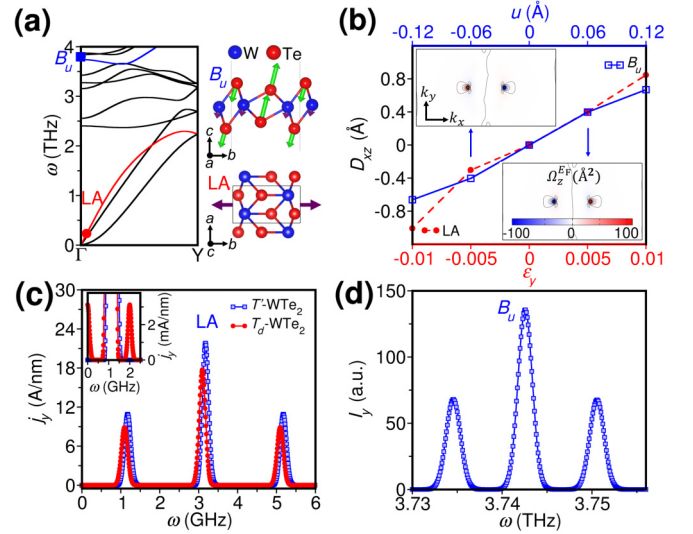


FIG. 2. GQuES-based transport spectroscopy of the WTe₂ monolayer. Phonon dispersion (a) of T' -WTe₂ monolayer (ML) with GQuES-active optical phonon B_u at $\omega_0 = 3.74$ THz (blue symbol) and longitudinal acoustic (LA) mode at $\omega_0 = \frac{2\pi}{L}v_g$ (red symbol) that constitutes a natural vibration of a sample of lateral size L . These vibrations [given in the right subpanel of (a)] dynamically lower the symmetry and induce a linear variation in D_{xz} with amplitude u of the B_u mode (blue solid line) and uniaxial strain ϵ_y , corresponding to the LA mode (red dashed line). The insets in (b) show contour plots of $\Omega_z(\mathbf{k})$ of T' -WTe₂ ML, exhibiting a reversal of the polarity of D_{xz} with $u < 0$ and $u > 0$. GQuES vibrational spectra from the measurement of NLH current $j_y(\omega)$ (c) and THz emission $I_y(\omega)$ (d) in response to voltage $V_x(\omega_{ac})$ applied to WTe₂. Macroscopic strain mode of vibration of T' -WTe₂ (blue squares) and T_d -WTe₂ (red circles) monolayered samples of lateral size $L = 4 \mu\text{m}$, corresponding to their LA phonons at $\omega_0 = 3.17$ GHz and $\omega_0 = 3.09$ GHz, respectively, manifests as three peaks (c) at ω_0 and $\omega_0 \pm 2\omega_{ac}$ ($\omega_{ac} = 1$ GHz). Additional peaks at $\omega = 0$ and $2\omega_{ac}$ are evident in the NLH current of T_d -WTe₂ [inset of (c)] due to its intrinsic D_{xz} . For $\omega_{ac} = 4$ GHz, the B_u mode of T' -WTe₂ ML manifests as peaks in $I_y(\omega)$ of emitted radiation (d) at $\omega_0 = 3.742$ THz and $\omega = \omega_0 \pm 2\omega_{ac}$.

direction lowers the lattice symmetry of T' -WTe₂. We now present the GQuES spectra of WTe₂, corresponding to the LA mode in GHz [Fig. 2(c)] and the B_u mode in THz [Fig. 2(d)], that may be validated with experimental observations in the transport mode. The signal is read as either a Hall current [Fig. 1(c)] or emitted THz radiation [Fig. 1(d)]. The precise frequency of the natural vibration is that of the LA mode at $q = \frac{\pi}{L}$ [Fig. 2(a), L being the sample width], which can be measured from the peaks in the ω -dependent Hall voltage at $\omega = \omega_0$ and $\omega_0 \pm 2\omega_{ac}$ [Fig. 2(c)] for a probing field of 1 GHz (ω_{ac}). In addition, we expect small peaks at $\omega = 0, 2\omega_{ac}$ for the noncentrosymmetric T_d -WTe₂ [inset of Fig. 2(c)] due to its intrinsic D (see Supplemental Material [16]), which permit characterization of the inversion asymmetry of the structure. For a field frequency of 4 GHz, the optical phonon B_u of T' -WTe₂ manifests as three peaks (centered at its frequency $\omega_0 = 3.74$ THz) in the intensity of emitted THz radiation [Fig. 2(d)] polarized along the y direction. The GQuES spectra can be systematically controlled by the frequency ω_{ac} of the driving field.

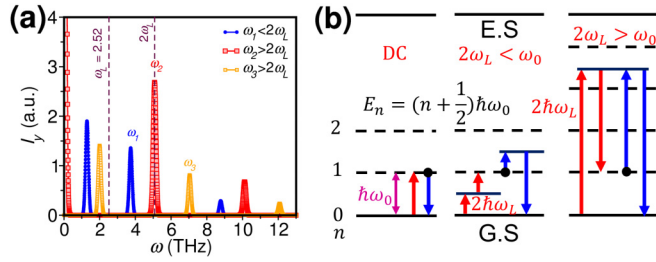


FIG. 3. GQuES-based optical spectroscopy of the WTe_2 monolayer. For a laser probe at frequency $\omega_L = 2.52$ THz polarized along the x axis, GQuES-active B_u phonons of T' - WTe_2 monolayer ($\omega_1 = 3.74$ THz, $\omega_2 = 5.08$ THz, $\omega_3 = 7.04$ THz) manifest as peaks at $\omega = \omega_0, 2\omega_L \pm \omega_0$ (blue symbol) and at $\omega = \omega_0, \omega_0 \pm 2\omega_L$ (red and yellow squares) in the emitted radiation $I_y(\omega)$ (a). Schematics of the quantum picture of GQuES (b) for rectification (dc), transport ($2\omega_L < \omega_0$), and emission ($2\omega_L > \omega_0$) modes. Solid and dashed black lines represent electronic and vibrational levels, respectively. Red and blue arrows denote generation and absorption of a phonon.

GQuES spectrum of the T' - WTe_2 monolayer obtained in the optical/emission mode [Fig. 1(e), with $\omega_L = 2.52$ THz] exhibits a rich structure of peaks associated with its three B_u modes [Fig. 3(a)]. While the transport mode requires electrical contacts for measurements, the THz/emission mode is contactless. While Stokes and anti-Stokes peaks in a Raman spectrum are centered at $\omega = \omega_L$, the peaks manifested in the GQuES spectra are centered at $\omega = 2\omega_L$ for $2\omega_L > \omega_0$, as illustrated by the quantum schematic in Fig. 3(b). At higher frequencies $\hbar\omega_L > E_g$ (see Supplemental Material [16]), we expect quantum resonant processes to become relevant and make the GQuES spectra even richer, requiring a full quantum mechanical analysis.

IV. SUBSTRATE-BASED GQuES

For GQuES spectroscopic signatures to be observable in a 2D crystal, (a) the condition of low crystal symmetry needs to be satisfied and (b) $\Omega_z(\mathbf{k})$ of electronic bands needs to be nonzero at the energies in the vicinity of the chemical potential. For example, hexagonal boron nitride (hBN) is a wide-gap insulator, commonly used in devices based on two-dimensional materials [39]. Its large band gap weakens the Hall responses, even if nonzero D is permitted by the dynamically lowered symmetries of the hBN crystal. These limitations, we show, can be overcome by aligning it on graphene, as shown in Fig. 4(a). A monolayer of graphene aligned with h-BN in the AB stacking (aligned gr-hBN) exhibits a narrow band gap of 45 meV at the Dirac points due to the interlayer crystal field. The point group symmetry $C_{3v}(E, C_{3z}, \sigma_x)$ of aligned gr-hBN allows its $\Omega_z(\mathbf{k})$ to be nonzero, but its intrinsic D vanishes due to threefold rotational symmetry.

Hexagonal BN exhibits a GQuES-active vibrational mode E at $\omega_0 = 41.9$ THz [Fig. 4(b)] that lowers its C_{3z} symmetry and its interaction with graphene modulates the electronic structure near the Dirac points of graphene inducing oscillations in D [Fig. 4(c)]. The activity of the E mode of hBN can be thus observed in the GQuES spectrum in the emission mode with ω -dependent I_y^ω emitted by the supporting antenna

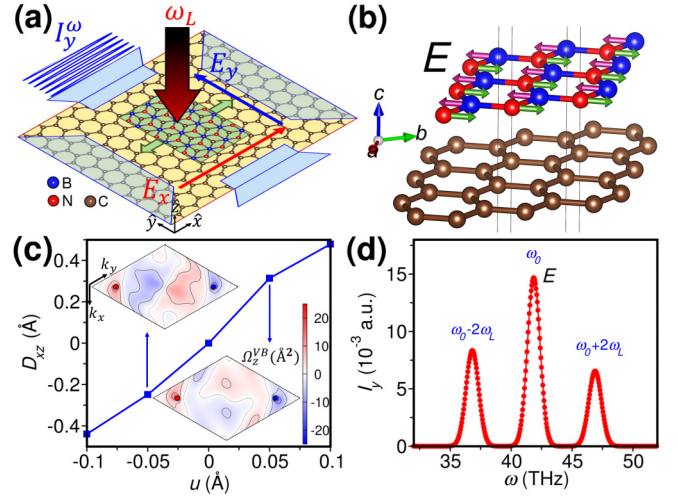


FIG. 4. Substrate-induced GQuES activity of phonons in aligned gr-hBN. (a) Schematics of an experimental setup for the observation of emission of THz radiation I_y^ω as the nonlinear Hall response to incident laser ω_L (black beam) due to substrate-induced GQuES activity of phonons in aligned gr-hBN. (b) The GQuES-active vibrational mode E (doubly degenerate at $\omega_0 = 41.9$ THz) of hBN lowers the structural symmetry and induces oscillating $D_{xz} \propto D'u \cos(\omega_0 t)$, where D' is given by the slope of variation in D_{xz} with u (c), the amplitude of the E mode. Inset in (c) are the contour plots of $\Omega_z(\mathbf{k})$ of aligned gr-hBN distorted with $u < 0$ and $u > 0$, whose asymmetry generates D . In response to an incident laser at $\omega_L = 2.52$ THz ($\lambda_L = 118.9 \mu\text{m}$) polarized along the x axis [red arrow in (a)], the E mode with vibration localized on hBN (b), manifests as peaks in the GQuES spectrum at $\omega = \omega_0 \pm 2\omega_L$ and $\omega = \omega_0$ in the emitted radiation $I_y(\omega)$ (d), polarized along the y direction [blue arrow in (a)] due to the nontrivial geometry of electronic states near the Dirac points of graphene (GQuES-inert material).

[Fig. 4(a)] in response to incident laser at $\omega_L = 2.52$ THz. The E mode manifests itself as a peak at $\omega_0 = 41.9$ THz along with side peaks at $\omega = 41.9 \pm 5.04$ THz in I_y^ω of emitted IR radiation [Fig. 4(d)].

V. DISCUSSION

We note that a spectroscopic (particularly vibrational) analysis typically involves an inverse problem: going from a spectrum to vibrational excitations and then to the identity (Hamiltonian) of a system. While the inverse may not even exist (nonunique mapping), spectroscopies work as powerful tools because vibrational frequencies indeed are often the fingerprints of a system. We thus expect GQuES to be quite practical as a tool for the analysis of vibrational spectra providing information complementary to other techniques.

The mechanism of GQuES-based vibrational spectroscopy originates from the oscillations in the quantum geometry of the electronic structure, and is applicable in graphene and MoS_2 -based 2D materials, where strain-dependent D has been reported [40–43]. The GQuES tool can be useful in translating signals in GHz or sub-GHz frequencies into those in the THz range [Fig. 2(d)], with a suitable choice of active material and modes of natural vibration. Our results in Fig. 4 show that

a GQuES-active material could be used as a substrate in the analysis of a system that is otherwise inert [Fig. 4(a)]. The GQuES vibrational spectroscopy demonstrated here with 2D crystals can be generalized to (a) other excitations that dynamically break the crystal symmetry, and (b) 3D crystals, opening up manifestations of quantum geometry in even richer set of phenomena.

VI. SUMMARY

In summary, we have demonstrated from first principles that lattice vibrations can be gauged using the characteristic oscillations they induce in the quantum geometry and Hall transport of electrons. We expect this to translate into power-

ful experimental techniques to measure the spectra of acoustic and optic phonons and other excitations.

ACKNOWLEDGMENTS

B.R. acknowledges SASTRA Deemed University, Thanjavur for financial assistance through a fellowship. U.V.W. acknowledges support from a JC Bose National Fellowship of SERB-DST, Government of India.

The idea was conceived through discussions between B.R. and U.V.W., the calculations were performed by B.R., a strong connection with experimental specifics was achieved through interactions between M.M.D., B.R., and U.V.W., and the manuscript was written by all three authors.

-
- [1] M. V. Berry, Quantal phase factors accompanying adiabatic changes, *Proc. R. Soc. London, Ser. A* **392**, 45 (1984).
- [2] D. Xiao, M.-C. Chang, and Q. Niu, Berry phase effects on electronic properties, *Rev. Mod. Phys.* **82**, 1959 (2010).
- [3] M. Z. Hasan and C. L. Kane, *Colloquium*: Topological insulators, *Rev. Mod. Phys.* **82**, 3045 (2010).
- [4] N. P. Armitage, E. J. Mele, and A. Vishwanath, Weyl and Dirac semimetals in three-dimensional solids, *Rev. Mod. Phys.* **90**, 015001 (2018).
- [5] R. Karplus and J. M. Luttinger, Hall effect in ferromagnetics, *Phys. Rev.* **95**, 1154 (1954).
- [6] J. Ye, Y. B. Kim, A. J. Millis, B. I. Shraiman, P. Majumdar, and Z. Tešanović, Berry phase theory of the anomalous Hall effect: Application to colossal magnetoresistance manganites, *Phys. Rev. Lett.* **83**, 3737 (1999).
- [7] I. Sodemann and L. Fu, Quantum nonlinear Hall effect induced by Berry curvature dipole in time-reversal invariant materials, *Phys. Rev. Lett.* **115**, 216806 (2015).
- [8] Q. Ma, S.-Y. Xu, H. Shen, D. MacNeill, V. Fatemi, T.-R. Chang, A. M. Mier Valdivia, S. Wu, Z. Du, C.-H. Hsu, S. Fang, Q. D. Gibson, K. Watanabe, T. Taniguchi, R. J. Cava, E. Kaxiras, H.-Z. Lu, H. Lin, L. Fu, N. Gedik *et al.*, Observation of the nonlinear Hall effect under time-reversal-symmetric conditions, *Nature (London)* **565**, 337 (2019).
- [9] Q. Ma, A. G. Grushin, and K. S. Burch, Topology and geometry under the nonlinear electromagnetic spotlight, *Nat. Mater.* **20**, 1601 (2021).
- [10] Y. Liu, X. Duan, H.-J. Shin, S. Park, Y. Huang, and X. Duan, Promises and prospects of two-dimensional transistors, *Nature (London)* **591**, 43 (2021).
- [11] S. Wang, X. Liu, and P. Zhou, The road for 2D semiconductors in the silicon age, *Adv. Mater.* **34**, 2106886 (2022).
- [12] Y. Liu, Y. Huang, and X. Duan, Van der Waals integration before and beyond two-dimensional materials, *Nature (London)* **567**, 323 (2019).
- [13] C. Liu, H. Chen, S. Wang, Q. Liu, Y.-G. Jiang, D. W. Zhang, M. Liu, and P. Zhou, Two-dimensional materials for next-generation computing technologies, *Nat. Nanotechnol.* **15**, 545 (2020).
- [14] D. J. Thouless, M. Kohmoto, M. P. Nightingale, and M. den Nijs, Quantized Hall conductance in a two-dimensional periodic potential, *Phys. Rev. Lett.* **49**, 405 (1982).
- [15] J. E. Moore and J. Orenstein, Confinement-induced Berry phase and helicity-dependent photocurrents, *Phys. Rev. Lett.* **105**, 026805 (2010).
- [16] See Supplemental Material at <http://link.aps.org/supplemental/10.1103/PhysRevB.110.014305> for additional frequency-dependent Hall responses of 2D materials due to a symmetry-permitted Berry curvature dipole, which includes Refs. [17–28].
- [17] P. Giannozzi, S. Baroni, N. Bonini, M. Calandra, R. Car, C. Cavazzoni, D. Ceresoli, G. L. Chiarotti, M. Cococcioni, I. Dabo, A. D. Corso, S. de Gironcoli, S. Fabris, G. Fratesi, R. Gebauer, U. Gerstmann, C. Gougoussis, A. Kokalj, M. Lazzeri, L. Martin-Samos *et al.*, QUANTUM ESPRESSO: A modular and open-source software project for quantum simulations of materials, *J. Phys.: Condens. Matter* **21**, 395502 (2009).
- [18] J. P. Perdew, K. Burke, and M. Ernzerhof, Generalized gradient approximation made simple, *Phys. Rev. Lett.* **78**, 1396(E) (1997).
- [19] S. Grimme, Semiempirical GGA-type density functional constructed with a long-range dispersion correction, *J. Comput. Chem.* **27**, 1787 (2006).
- [20] X. Wang, J. R. Yates, I. Souza, and D. Vanderbilt, *Ab initio* calculation of the anomalous Hall conductivity by Wannier interpolation, *Phys. Rev. B* **74**, 195118 (2006).
- [21] A. A. Mostofi, J. R. Yates, G. Pizzi, Y.-S. Lee, I. Souza, D. Vanderbilt, and N. Marzari, An updated version of wannier90: A tool for obtaining maximally-localised Wannier functions, *Comput. Phys. Commun.* **185**, 2309 (2014).
- [22] Q. Wu, S. Zhang, H.-F. Song, M. Troyer, and A. A. Soluyanov, WannierTools: An open-source software package for novel topological materials, *Comput. Phys. Commun.* **224**, 405 (2018).
- [23] S. S. Tsirkin, High performance Wannier interpolation of Berry curvature and related quantities with WannierBerri code, *npj Comput. Mater.* **7**, 33 (2021).
- [24] Wolfram Research, Inc., Mathematica, Version 12.0, Champaign, IL, 2019, <https://www.wolfram.com/mathematica>.
- [25] M. N. Ali, J. Xiong, S. Flynn, J. Tao, Q. D. Gibson, L. M. Schoop, T. Liang, N. Haldolaarachchige, M. Hirschberger, N. P. Ong, and R. J. Cava, Large, non-saturating magnetoresistance in WTe_2 , *Nature (London)* **514**, 205 (2014).

- [26] C. R. Dean, A. F. Young, I. Meric, C. Lee, L. Wang, S. Sorgenfrei, K. Watanabe, T. Taniguchi, P. Kim, K. L. Shepard, and J. Hone, Boron nitride substrates for high-quality graphene electronics, *Nat. Nanotechnol.* **5**, 722 (2010).
- [27] Y. Kim, Y. I. Jhon, J. Park, J. H. Kim, S. Lee, and Y. M. Jhon, Anomalous Raman scattering and lattice dynamics in mono- and few-layer WTe_2 , *Nanoscale* **8**, 2309 (2016).
- [28] R. J. Nemanich, S. A. Solin, and R. M. Martin, Light scattering study of boron nitride microcrystals, *Phys. Rev. B* **23**, 6348 (1981).
- [29] Y. Zhang, Y. Sun, and B. Yan, Berry curvature dipole in Weyl semimetal materials: An *ab initio* study, *Phys. Rev. B* **97**, 041101(R) (2018).
- [30] C.-L. Zhang, T. Liang, Y. Kaneko, N. Nagaosa, and Y. Tokura, Giant Berry curvature dipole density in a ferroelectric Weyl semimetal, *npj Quantum Mater.* **7**, 107 (2022).
- [31] Z. Z. Du, C. M. Wang, H.-Z. Lu, and X. C. Xie, Band signatures for strong nonlinear Hall effect in bilayer WTe_2 , *Phys. Rev. Lett.* **121**, 266601 (2018).
- [32] S.-Y. Xu, Q. Ma, H. Shen, V. Fatemi, S. Wu, T.-R. Chang, G. Chang, A. M. M. Valdivia, C.-K. Chan, Q. D. Gibson, J. Zhou, Z. Liu, K. Watanabe, T. Taniguchi, H. Lin, R. J. Cava, L. Fu, N. Gedik, and P. Jarillo-Herrero, Electrically switchable Berry curvature dipole in the monolayer topological insulator WTe_2 , *Nat. Phys.* **14**, 900 (2018).
- [33] Y. Gao, S. A. Yang, and Q. Niu, Field induced positional shift of Bloch electrons and its dynamical implications, *Phys. Rev. Lett.* **112**, 166601 (2014).
- [34] H. Liu, J. Zhao, Y.-X. Huang, W. Wu, X.-L. Sheng, C. Xiao, and S. A. Yang, Intrinsic second-order anomalous Hall effect and its application in compensated antiferromagnets, *Phys. Rev. Lett.* **127**, 277202 (2021).
- [35] R. Loudon and N. Kurti, Theory of the first-order Raman effect in crystals, *Proc. R. Soc. London, Ser. A* **275**, 218 (1963).
- [36] S. Tang, C. Zhang, D. Wong, Z. Pedramrazi, H.-Z. Tsai, C. Jia, B. Moritz, M. Claassen, H. Ryu, S. Kahn, J. Jiang, H. Yan, M. Hashimoto, D. Lu, R. G. Moore, C.-C. Hwang, C. Hwang, Z. Hussain, Y. Chen, M. M. Ugeda *et al.*, Quantum spin Hall state in monolayer $1T'$ - WTe_2 , *Nat. Phys.* **13**, 683 (2017).
- [37] A. A. Soluyanov, D. Gresch, Z. Wang, Q. Wu, M. Troyer, X. Dai, and B. A. Bernevig, Type-II Weyl semimetals, *Nature (London)* **527**, 495 (2015).
- [38] D. Shin, A. Rubio, and P. Tang, Light-induced ideal Weyl semimetal in HgTe via nonlinear phononics, *Phys. Rev. Lett.* **132**, 016603 (2024).
- [39] J. D. Caldwell, I. Aharonovich, G. Cassabois, J. H. Edgar, B. Gil, and D. N. Basov, Photonics with hexagonal boron nitride, *Nat. Rev. Mater.* **4**, 552 (2019).
- [40] S. Sinha, P. C. Adak, A. Chakraborty, K. Das, K. Debnath, L. D. V. Sangani, K. Watanabe, T. Taniguchi, U. V. Waghmare, A. Agarwal, and M. M. Deshmukh, Berry curvature dipole senses topological transition in a moiré superlattice, *Nat. Phys.* **18**, 765 (2022).
- [41] R. Battilomo, N. Scopigno, and C. Ortix, Berry curvature dipole in strained graphene: A Fermi surface warping effect, *Phys. Rev. Lett.* **123**, 196403 (2019).
- [42] R.-C. Xiao, D.-F. Shao, Z.-Q. Zhang, and H. Jiang, Two-dimensional metals for piezoelectriclike devices based on Berry-curvature dipole, *Phys. Rev. Appl.* **13**, 044014 (2020).
- [43] J. Son, K.-H. Kim, Y. H. Ahn, H.-W. Lee, and J. Lee, Strain engineering of the Berry curvature dipole and valley magnetization in monolayer MoS_2 , *Phys. Rev. Lett.* **123**, 036806 (2019).